

Traveltimes and amplitudes of seismic waves: a re-assessment

Guust Nolet, F.A. Dahlen and Raffaella Montelli

Department of Geosciences, Princeton University, Princeton NJ.

Abstract

In this paper we give a simplified derivation of the sensitivity of travel time measurements by cross-correlation and of amplitudes of body waves to the seismic velocity structure in the Earth, taking into account the effect of finite frequencies. We introduce a new technique to compute kernels in 3D media, using graph theory and ray bending. We show that the finite-frequency sensitivity kernels (or ‘banana-doughnut’ kernels) are sizeable even for local studies done at very high frequencies, e.g. in refraction surveys. We conclude that it is advisable to apply finite-frequency theory to most, if not all, modern seismic surveys.

1. Introduction

Travel time measurements have been the backbone of seismology since the earliest seismographs showed P and S waves preceding the more dominant surface waves near the end of the 19th century (Bates et al., 1982). Since then, generations of seismologists have been occupied with picking arrival times from smoked paper or photographic records.

In recent times, the proliferation of digital recordings has changed that. Cross-correlation methods (VanDecar and Crosson, 1990) have replaced manual picking, and enable us to measure travel times accurately even from long period seismograms (Woodward and Masters, 1991). Because of their excellent signal-noise ratio, long period records often yield more stable travel time measurements, and offer an attractive addition to short-period arrival times.

Theory, on the other hand, has been slower to catch up. The onset of a body wave from a short-period seismogram represents a travel time at fairly high frequency, usually well within the range of validity of the approximation of geometrical optics. This approximation assumes that the seismic energy travels along ‘rays’ that are very much thinner than the size of heterogeneities in the medium.

The limitations of the ray approximation gained attention when broadband sensors became more prevalent (Wielandt, 1987; Nolet, 1992; Cervený and Soares, 1992; Nolet et al., 1994; Woodward, 1993; Yomogida, 1992), but much of the interpretation of seismic arrival times, be it for earthquake location or for imaging, is still beholden to the assumptions that the wavelength of the seismic waves is small both with respect to the scale length of heterogeneities and with respect to the length of the ray itself. These limitations have become restrictive as the number and the quality of broadband data have quickly improved and measurements were more generally done at longer periods. A compressional or P wave with a period of 20 seconds has a wavelength of 260 km in the lower mantle - far larger than the thickness of a slab fragment and probably larger than the typical width of a plume. Such small sized heterogeneities may have a very much reduced influence on the time of the first arriving seismic energy, even though they influence the waveshape.

One could try to invert for *waveform distortions* rather than for *travel time* anomalies when interpreting long period seismograms. This, however, introduces its own complications. Early waveform inver-

sion techniques relied on the summation of surface wave modes to generate body waves such as SS and SSS (Nolet et al., 1986; Nolet 1990). But classical surface wave theory assumes a layer-cake structure for the Earth, and to take full account of lateral heterogeneity one must incorporate mode coupling effects (Li and Tanimoto, 1993; Li and Romanowicz, 1995; Marquering et al., 1996). This makes waveform inversions computationally intensive.

Marquering et al. (1999) recognized that the delay times obtained by cross-correlation are the more suitable, discrete data to invert for. They still used surface-wave mode summation to calculate the change in waveform that affects the cross-correlation, which made an application to large data sets infeasible. Dahlen et al. (2000) abandoned the mode summation approach and computed the change in waveform using rays that reflect from heterogeneities (Figure 1). In its most efficient variant, paraxial rays are substituted for exactly traced rays. Thus, we obtain the necessary computational efficiency using ray theory to circumvent the limitations of ray theory: the assumption of infinite frequency has been replaced by the less drastic approximation of *single scattering*.

In this paper we shall closely follow Dahlen et al. (2000), though we shall attempt to give this paper a more tutorial flavour, concentrating on concepts rather than a full development of the theory. A new element in the present paper is the use of graph theory for the computation of the travel times and amplitudes of scattered waves, rather than the paraxial approximation. This makes the method more easily applicable in media where the background model is already laterally heterogeneous, since it avoids the problems of two-point ray tracing.

2. Heuristic introduction of banana-doughnut kernels

We develop our ideas using the simple cartoon of Figure 2. In this figure, the direct wave from source s to receiver r arrives together with a scattered wave that arrives with a slight delay. The sign of the delayed wave is determined by the sign of the velocity anomaly that causes the scattered wave: fast anomalies generate scattered waves with a negative polarity. Figure 2 shows the two possible effects of this in the seismogram. $u(t)$ denotes the seismogram in an unperturbed medium. If the seismogram is composed of the direct wave plus a scattered wave $\delta u(t)$ from a slow velocity anomaly (generating a scatterer

with a positive polarity as in the bottom of Figure 2), the maximum of the cross-correlation $C(t)$ is delayed. Clearly, the onset of the observed wavelet $u(t) + \delta u(t)$ is not affected, in agreement with the common assumption that onsets are dominated by very high frequencies, such that ray theory is valid. The situation in the top part of Figure 2 is the reverse: the scatterer is now fast, the polarity of the scattered wave negative, and the cross-correlation shows a time advance.

These two figures show the basic ideas of finite frequency seismology: scatterers off the ray path may not influence the *onset* of the wave, but they do advance or delay the full waveform. Cross-correlation methods that use all or part of the waveform to determine the travel time delay, are sensitive to these waveform effects. To be consistent, travel time data derived from cross correlation should therefore not be inverted with methods based on ray theory.

A second phenomenon, which is rather counter-intuitive, is that a small scatterer on the raypath does not change the shape of the waveform but only perturbs its amplitude. This situation is depicted in Figure 3. The reason is that the scattered wave $\delta u(t)$ in this case is not delayed (the sum of its paths to and from the scatterer equals the original raypath). The delay incurred by the scattered wave is essential to influence the travel time of the wave. Thus, scattering objects must be located away from the actual ray to be seen in a tomographic inversion. Of course, large objects always extend beyond the direct vicinity of a ray and therefore do influence the travel time, conforming to our ray-theoretical intuition. But a small pebble will only be seen if it is *not* on the ray!

In Figures 2 and 3 we assumed that $\delta u(t)$ preserves the shape of $u(t)$, i.e. there is no phase shift. But once the wave has passed a focal point or caustic, the wave energy defocuses again. Theory tells us that a wave acquires a $\pi/2$ phase shift upon passage through a caustic and a shift of π upon passage through a three-dimensional focal point. The latter case reverses the sign of the added scattered wave, and may turn a delay into an advance. Focal points are rare if not entirely absent in seismology, but a $\pi/2$ shift is quite common in a layered Earth, or for surface reflections like PP waves. We shall see that such a phase shift has a complicated effect on the resulting delay of the wave.

The upshot of this all is that the delay time measured by cross-correlation is not just a function of the anomalies encountered on the geometrical ray between source and receiver, but in a volume around

it. The volume is finite, because a wave that arrives too late to be included in the cross-correlation window clearly has no influence on the measured delay time. If the ray is straight, as in the homogeneous medium depicted in Figure 1, the volume including all timely scatterers is given by an ellipse. In more realistic media where the geometrical ray is bent, the volume resembles that of a banana. Since the sensitivity is zero on the geometrical ray itself if there is no caustic phase shift, the sensitivity kernel ('Frechet kernel' in the mathematical jargon) has a hole in the center. Marquering et al. (1999) therefore named these kernels 'banana-doughnut kernels'. For an example of such a kernel in global seismology, take a look at Figure 4.

The net effect of wavefront healing is that delays spread out over the wavefront, and diminish in magnitude as the wave progresses along the raypath (Nolet and Dahlen, 2000; Hung et al., 2001). This phenomenon is frequency and wavelength dependent as shown in Figure 5. For infinite frequencies, or infinitely small wavelength, it will be negligible at finite distance from the anomaly. As the wavelength grows to a length comparable to the dimension of the anomaly, the wavefront healing becomes significant even at short distances from the anomaly.

One last caveat: the theory as described here is a single scattering theory that is fully linear. As such it predicts that the magnitude of a delay is proportional to the amplitude of the anomaly. In particular, fast and slow anomalies of equal magnitude are predicted to have delay times that are equal in magnitude, they only differ in sign. While correct to first order, there is a second order effect that does introduce asymmetry, as pointed out by Wielandt (1987). A fast anomaly will advance the wavefront, and this advanced wavefront will propagate without further interference. Thus, negative delay times do not 'heal'. A slow anomaly, on the other hand, creates a delayed wavefront with an unperturbed zone that may be filled in by energy radiating from the sides (using Huygens' Principle). Nolet and Dahlen (2000) showed that the situation is more complicated than that, however: the advanced wavefront loses energy quickly, and a negative delay will at first retain its magnitude (or even grow!), but as it spreads its energy too thinly, at some point the wave amplitude will become very small and in practice drown in the noise.

3. Travel time delays

It is now time to translate the heuristic ideas of the previous section into a quantitative theory. In the limit of weak scattering, we may use the ray approximation to build a theory that extends beyond the limitations of ray theory itself. This may seem circular or magical, but it actually works, as was convincingly shown in numerical simulations by Hung et al. (2000).

We assume that the velocity in the Earth can be represented by a smoothly varying background model for which ray theory is valid, and to which heterogeneity is added that acts to scatter a (small) fraction of the wave energy. As in Figure 1, the signal in the receiver consists of a direct ray arrival $u(t)$ and a scattered ray arrival $\delta u(t)$. For a point scatterer (i.e. a scatterer of a size very much smaller than the dominant wavelength of the wave), the waveshape of the scattered wave will be identical to that of the direct wave, but it will be delayed by a delay τ , and it will only have a fraction ϵ of the original amplitude:

$$g(t, \mathbf{x}) = \epsilon(\mathbf{x})u(t - \tau) \quad (1)$$

where we used the notation g to indicate the scatterer is a point response or Green's function. (1) assumes there are no caustic phase shifts along the paths travelled to and from the scatterer. Such shifts could easily be handled by adding a Hilbert transform or $(-)$ sign to (1), but we shall in this paper only deal with the simple case of first arrivals which never have caustic phase shifts. It also assumes that we can neglect P \rightarrow S and S \rightarrow P scattering, which is appropriate because the converted waves arrive with a very large time advance or delay unless the scatterer is near the source.

For scatterers of realistic dimension, we can compute δu using ray theory by a summation of point scatterers:

$$\delta u(t) = \int \epsilon(\mathbf{x})u(t - \tau)d^3\mathbf{x} \quad (2)$$

How does δu influence the travel time? The autocorrelation of the unperturbed seismogram $u(t)$ is given by:

$$\gamma(t) = \int u(t' - t)u(t') dt' \quad (3)$$

We define the travel time delay by the maximum of the cross-correlation function of the observed signal

$u + \delta u$ with the unperturbed wave u :

$$\gamma(t) + \delta\gamma(t) = \int u(t' - t)[u(t') + \delta u(t')] dt' \quad (4)$$

For the unperturbed wave, the cross-correlation reaches its maximum at zero lag, so:

$$\dot{\gamma}(0) = 0 \quad (5)$$

and for the perturbed wave the maximum is reached after a delay δT :

$$\dot{\gamma}(\delta T) + \delta\dot{\gamma}(\delta T) = 0 \quad (6)$$

where the dot denotes time differentiation. Developing $\dot{\gamma}$ to first order, we find (Luo and Schuster 1991; Marquering et al., 1999):

$$\dot{\gamma}(\delta T) + \delta\dot{\gamma}(\delta T) = \dot{\gamma}(0) + \ddot{\gamma}(0)\delta T + \delta\dot{\gamma}(0) + \mathcal{O}(\delta^2) = 0 \quad (7)$$

or using (5) and (3):

$$\delta T = -\frac{\delta\dot{\gamma}(0)}{\ddot{\gamma}(0)} = -\frac{\int_{-\infty}^{\infty} \dot{u}(t)\delta u(t)dt}{\int_{-\infty}^{\infty} \ddot{u}(t)u(t)dt} \quad (8)$$

We get u by computing a synthetic signal for the background model. This introduces a number of complications — such as uncertainties in the source location and excitation as well as in the attenuation along the path — that we shall ignore here. Equation (8) is in the time domain, and could in principle be used to compute the sensitivity kernel for velocity perturbations δc by expressing $\epsilon(\mathbf{x})$ in (2) in terms of the δc . However, to avoid that we have to perform both a volume integration over \mathbf{x} and a convolution over scatterer delays τ , it is more convenient to express (8) in the frequency domain. Using Parseval's theorem and the spectral property of real signals $u(-\omega) = u(\omega)^*$, where an asterisk denotes the complex conjugate:

$$\delta T = \frac{\text{Re} \int_0^{\infty} i\omega u(\omega)^* \delta u(\omega) d\omega}{\int \omega^2 u(\omega)^* u(\omega) d\omega} \quad (9)$$

4. Born theory for seismic waves

In this section we shall express δu in terms of the P and S velocity perturbations $\delta\alpha$ and $\delta\beta$. We shall denote the signed amplitude of δu by $\delta\bar{u}$ ($\delta\bar{u}$ is the wave stripped of its phase delay due to propagation, but retaining any sign changes acquired upon scattering). This amplitude is defined by the scattering strength $\epsilon(\mathbf{x})$ in (1) and (2). For a full development of the theory of single scatterers, we refer to Dahlen et

al. (2000) or the references therein, especially Wu and Aki (1985). For this paper, we shall take a simplified, more tutorial approach. In particular, we assume that the coefficient for forward scattering at an angle $\theta = 0$ is valid for all angles. The reason is that scattering at large angles almost always implies a large delay of the scattered wave, making an interference within a narrow time window such as sketched in Figure 2 impossible. In particular we neglect:

- mode conversions upon scattering
- scattering from density perturbations
- the angle dependence of scattering

For example, the amplitude of a scattered wave from a small volume dV with perturbations in density $\delta\rho$ and in Lamé parameters $\delta\lambda$ and $\delta\mu$, for P→P scattering from an incoming wave of amplitude 1 is given by (Wu and Aki, 1985):

$$\delta\bar{u}^{PP}(\omega) = \frac{\omega^2}{4\pi\alpha^2} \frac{1}{r} \left[\frac{\delta\rho}{\rho} \cos\theta - \frac{\delta\lambda}{\lambda + 2\mu} - 2\frac{\delta\mu}{\lambda + 2\mu} \cos\theta^2 \right] dV \quad (10)$$

where θ is the scattering angle, ρ the density, α the P velocity and λ and μ Lamé's elastic parameters. For purely forward scattering ($\theta = 0$) this gives:

$$\begin{aligned} \delta\bar{u}^{PP}(\omega) &= \frac{\omega^2}{4\pi\alpha^2} \frac{1}{r} \left[\frac{\delta\rho}{\rho} - \frac{\delta\lambda}{\lambda + 2\mu} - 2\frac{\delta\mu}{\lambda + 2\mu} \right] dV \\ &= -\frac{\omega^2}{2\pi\alpha^2} \frac{1}{r} \frac{\delta\alpha}{\alpha} dV \end{aligned} \quad (11)$$

because

$$\frac{\delta\rho}{\rho} - \frac{\delta\lambda + 2\delta\mu}{\lambda + 2\mu} = -2\frac{\delta\alpha}{\alpha} \quad (12)$$

The factor $-\omega^2/2\pi\alpha^2$ is denoted as the scattering coefficient \mathcal{S}_α^{PP} , where the subscript indicates the type of heterogeneity. Note that the power $|\delta\bar{u}^{PP}|^2$ of the scattered wave is proportional to ω^4 ('Rayleigh scattering'). This high-pass filtering effect of a point-like scatterer compensates for the low-pass filtering effect of any integration over space to build the response of a large object. Table 1 in Dahlen et al. (2000) provides a convenient summary of all scattering coefficients. For this paper it is sufficient to note that, in the approximation of forward scattering:

$$\text{P} \rightarrow \text{P} : \quad \mathcal{S}_\alpha^{PP} = -\frac{\omega^2}{2\pi\alpha^2} \quad (13)$$

$$\text{S} \rightarrow \text{S} : \quad \mathcal{S}_\beta^{SS} = -\frac{\omega^2}{2\pi\beta^2} \quad (14)$$

all other scattering coefficients being 0. Although scattering of shear waves depends on the polarization of the wave, the expressions reduce to the same simple constant for forward scattering.

5. Sensitivity kernels at finite frequency

So far, we have made no assumptions about the nature of the zero order field $u(\omega)$. Clearly, the more accurate and complete the zero order field is, the more accurate our estimate of $\delta u(\omega)$. The method to use for the computation of $\delta u(\omega)$ is less critical since approximation errors will be of second order in $u(\omega) + \delta u(\omega)$.

As we discussed in the heuristic introduction, Zhao et al. (2000) construct both $\delta u(t)$ and $u(t)$ by summation of discrete normal modes ${}_n S_\ell^m$ and ${}_n T_\ell^m$ of the Earth, each with its own frequency ${}_n \omega_\ell^m$, a technique that finds its roots in the formalism developed for very low frequency waveforms by Woodhouse and Girnius (1982). More efficient — but still too cumbersome for large scale inversions — is the approach adopted by Marquering et al. (1999), who summed surface waves in the frequency domain for a equidistant set of frequencies of interest. Summation of modes has the advantage that every possible wave arrival in the time window of interest is represented in $u(\omega)$, even if it is a diffracted or evanescent wave. Dahlen et al. (2000) used what is probably the most efficient method and constructed u using ray theory. Moreover, they use a paraxial approximation to estimate the geometrical spreading \mathcal{R} as well as the travel time to the scattering point.

In this paper we shall also use ray theory, though we shall refrain from a paraxial approximation for the scattering detour time. Our simplified development uses several results from Aki and Richards (1980), Chapter 4, and we shall refer to equation numbers in that chapter using an indication 'AR'.

The spectrum of a far field P wave from a moment tensor source with time behaviour $m(t)$ in a homogeneous medium with velocity α_0 and density ρ_0 is (using AR 4.29):

$$u^P(\omega) = \frac{\mathcal{F}^P \dot{m}(\omega)}{4\pi\rho_0\alpha_0^3 r_{rs}} e^{-i\omega r_{rs}/\alpha_0} \quad (15)$$

where the geometrical spreading is given by the distance r_{rs} from the source s to the receiver r , and where \mathcal{F}^P denotes an amplitude factor that includes the radiation pattern. $\omega = 2\pi f$ is the frequency of the wave; $\dot{m}(t)$ is the derivative of $m(t)$ and $\dot{m}(\omega)$

is the Fourier transform of $\dot{m}(t)$. In a heterogeneous medium, the ‘ray approximation’ involves modeling the amplitude by a local factor $(\alpha_r \rho_r)^{-\frac{1}{2}} \mathcal{R}_{rs}^{-1}$, where \mathcal{R}_{rs} replaces r_{rs} as the geometrical spreading factor and where $(\alpha_r \rho_r)^{-\frac{1}{2}}$ models the effect of changes in impedance, such that the energy flux is conserved; in addition, the travel time is generalized from r/α_0 to T_{rs} . Fitting the remaining constants in this Ansatz to (15) near the source, where the two should agree, results in the generalized expression (cf. AR 4.88):

$$u(\omega) = \frac{\mathcal{F}^P \dot{m}(\omega)}{4\pi\alpha_s^2 \mathcal{R}_{rs} \sqrt{\rho_s \rho_r \alpha_s \alpha_r}} e^{-i\omega T_{rs}} \quad (16)$$

Thus, the effect of gradual changes in the medium is obtained by replacing:

$$\rho\alpha^3 r \rightarrow \alpha_s^2 \mathcal{R}_{rs} \sqrt{\rho_s \rho_r \alpha_s \alpha_r} \quad (17)$$

Replacing the source s with the scatterer x , we may use (17) to generalize the expression for the scattered wave (11) to heterogeneous media by adding the appropriate geometrical decay and a phase delay:

$$\delta u^{PP}(\omega) = -\frac{\omega^2 \rho_x dV}{2\pi \mathcal{R}_{rx} \alpha_x \sqrt{\alpha_x \alpha_r \rho_x \rho_r}} \left(\frac{\delta\alpha}{\alpha} \right)_x e^{-i\omega T_{rx}} \quad (18)$$

Computationally, it is very inefficient to have to calculate the geometrical spreading \mathcal{R}_{rx} for each possible scattering location x . However, if we compute the geometrical spreading from the receiver to every point in the model, the reciprocity principle gives us the spreading factor \mathcal{R}_{rx} from (Dahlen and Tromp, 1998, eq. 12.30):

$$\alpha_r \mathcal{R}_{xr} = \alpha_x \mathcal{R}_{rx} \quad (19)$$

If we replace the receiver r by a scatterer x , (16) can also be used to find the wavefield that impacts on a point scatterer. This gives us the necessary amplitude for the wave that impacts on the scatterer. Multiplying the scattered wave (11) with this amplitude, and applying (19) results in:

$$\delta u^{PP}(\omega) = -\frac{\mathcal{F}^P \dot{m}(\omega) \omega^2}{8\pi^2 \alpha_s^{5/2} \rho_s^{1/2} \alpha_r^{3/2} \rho_r^{1/2}} \frac{(\delta\alpha/\alpha)_x dV}{\alpha_x \mathcal{R}_{xs} \mathcal{R}_{xr}} e^{-i\omega(T_{rs}+T_{rx})} \quad (20)$$

We find the time delay induced by such a point scatterer if we insert (16) and (20) into the expression (9) for the cross-correlation time delay:

$$\delta T = \frac{(\delta\alpha/\alpha)_x dV}{2\pi\alpha_r\alpha_x} \frac{\mathcal{R}_{rs}}{\mathcal{R}_{xr}\mathcal{R}_{xs}} \frac{\text{Re} \int_0^\infty i\omega^3 |\dot{m}(\omega)|^2 e^{-i\omega\Delta T} d\omega}{\int_0^\infty \omega^2 |\dot{m}(\omega)|^2 d\omega} \quad (21)$$

where ΔT is the extra time needed for the ray to visit the scatterer x at \mathbf{x} :

$$\Delta T(\mathbf{x}) = T_{rs} - T_{xr} - T_{xs} \quad (22)$$

For a more general heterogeneity, we integrate over all point scatterers:

$$\delta T = \int K_\alpha(\mathbf{x}) \frac{\delta\alpha}{\alpha} dV \quad (23)$$

where $K_\alpha(\mathbf{x})$ is the Fréchet kernel (often named banana-doughnut kernel):

$$K_\alpha(\mathbf{x}) = -\frac{1}{2\pi\alpha_r\alpha_x} \frac{\mathcal{R}_{rs}}{\mathcal{R}_{xr}\mathcal{R}_{xs}} \frac{\int_0^\infty \omega^3 |\dot{m}(\omega)|^2 \sin[\omega\Delta T(\mathbf{x})] d\omega}{\int_0^\infty \omega^2 |\dot{m}(\omega)|^2 d\omega} \quad (24)$$

The sensitivity of an arrival time may deviate significantly from that predicted by geometrical ray theory, as is evident from their shape and width such as depicted in Figure 4. Montelli et al. (2004a) indeed demonstrate that the use of finite-frequency kernels has a significant influence on the amplitude of velocity anomalies in tomographic images from long period data, which can easily be amplified by as much as 50% or more. In fact, even ISC-derived travel time delays, often presumed to be representative of the travel times for very high frequency waves, may be in need of finite-frequency treatment, as a careful comparison of short- and long period delay times by Montelli (2003) has shown.

The use of banana-doughnut kernels in an inversion of teleseismic data enabled Montelli et al. (2004b) to invert jointly the short-period ISC delay times with long period travel times obtained by cross-correlation (Bolton and Masters, 2001), which was the first study to show convincingly that a large number of mantle plumes originate in the lowermost mantle.

We note that the simple expressions for amplitude and delay time inversion (24) and (21) have been derived using the far-field expressions for the seismic wavefield. This gives problems in the case the scatterer is located near the source or directly beneath the receiver. Though the singularity in the banana-doughnut kernels is integrable and may be handled by assuming a small region of constant velocity perturbation around it, (24) and (21) do not contain near- and intermediate field terms that may be important especially at low frequency. In an important contribution, Favier et al. (2004) develop finite frequency kernels for travel time perturbations in the near field, as well as for S-wave splitting observations.

6. Finite-frequency theory for amplitudes

Amplitudes of body waves undergo very similar wavefront healing effects. We define the amplitude of a body wave pulse of length T_p as:

$$A = \sqrt{\frac{1}{T_p} \int_0^{T_p} u^2(t) dt} \quad (25)$$

Following the same procedure that led to (9) one finds for the difference in amplitude between a synthetic pulse u and a perturbed pulse $u + \delta u$:

$$\frac{A_{obs} - A_{syn}}{A_{syn}} = \frac{\text{Re} \int_0^\infty u(\omega)^* \delta u(\omega) d\omega}{\int_0^\infty u(\omega)^* u(\omega) d\omega} \quad (26)$$

The amplitude kernel again follows from substitution of the expressions for the scattered waves (Dahlen and Baig, 2002):

$$\frac{A_{obs} - A_{syn}}{A_{syn}} = \int K_\alpha^{(A)}(\mathbf{x}) \frac{\delta\alpha}{\alpha} dV \quad (27)$$

$$K_\alpha^{(A)}(\mathbf{x}) = \frac{1}{2\pi\alpha_r\alpha_x} \frac{\mathcal{R}_{rs}}{\mathcal{R}_{xr}\mathcal{R}_{xs}} \frac{\int_0^\infty \omega^2 |\dot{m}(\omega)|^2 \cos[\omega\Delta T(\mathbf{x})] d\omega}{\int_0^\infty |\dot{m}(\omega)|^2 d\omega} \quad (28)$$

A close inspection of (28) shows that it differs by a factor ω from the expression (24) for the travel time (as expected because the amplitude datum is dimensionless), and by a cosine- rather than a sine-dependence on the extra travel time ΔT for the scattered wave. Thus, a scatterer located exactly on the ray, where $\Delta T = 0$, will have a maximum effect on amplitude (see Figure 3).

An additional advantage of using finite-frequency theory for amplitudes is the increased stability for body wave amplitude computations, where the forward problem is often hampered by minuscule triplifications of the wavefront in 3D media that may have little physical importance (Baig and Dahlen, 2003).

7. Application to Vesuvius

When we scale the teleseismic results to regional experiments, it is the ratio between the width w_F of the Fréchet kernel (or Fresnel zone) and the length of the ray that is of interest. This ratio is a function both of the frequency ω of the wave, through the relationship $\lambda = 2\pi\alpha/\omega$, as well as the length L of the

ray:

$$\frac{w_F}{L} = \frac{\sqrt{\lambda L}}{L} = \sqrt{\frac{2\pi\alpha}{\omega L}} \quad (29)$$

Since the ratio scales with ωL , a decrease in raylength by a factor of 100 would give Fréchet kernels of similar shape if the frequency is increased by this same factor. Thus, for local tomographic studies we may expect finite frequency effects if the dominant period of the waves is of the order of 0.1 s or more.

In addition, crustal or lithospheric structures are much more heterogeneous than the radially symmetric models such as PREM that we use for the computation of global kernels. Assuming a simple layered structure may then significantly misrepresent the true Earth, with the Fréchet kernels that do not correctly model the influence of diffracted wave energy on the delay time. In this section we shall use a more generally applicable method to compute Fréchet kernels. Here we only sketch the essentials of the method, a detailed account will be published elsewhere.

The most robust algorithm to compute travel times in complicated 3D structures is graph theory (Moser, 1991) which is guaranteed to find the absolute shortest time path for a ray that is forced to travel between nodes in a network, or *graph*. Because the ray is represented by straight line segments between nodes, its travel time is not very accurate and, because of Fermat's Principle, always an overestimate of the shortest time that is possible for an arbitrary ray. Moser et al.(1992) present a method to bend this ray, using the graph nodes as beta spline supports that can be moved around. We found that this approach may lead to convergence to different (but close) local minima for neighbouring rays in a pencil of rays, leading to small but short wavelength fluctuations in travel time T throughout the model. This can prove disastrous when computing the geometrical spreading (which is dependent on $\nabla^2 T$). A stabler bending can be effected by discarding the spline interpolation and using linear connections instead. The node locations x_i , y_i and z_i satisfy a set of linear equations if they are to minimize the total travel time, given by

$$T = \sum_{i=2}^N \frac{L_i}{\bar{v}_i} \quad (30)$$

for a ray consisting of N segments of length L_i , with average velocity $\bar{v}_i = \frac{1}{2}(v_i + v_{i-1})$. According to Fermat's principle $\partial T / \partial x_k = 0$ for $k = 2, \dots, N - 1$ (the

end nodes are fixed), and similarly for y_k and z_k :

$$\frac{\partial T}{\partial x_k} = \frac{\partial L_k}{\bar{v}_k \partial x_k} + \frac{\partial L_{k+1}}{\bar{v}_{k+1} \partial x_k} - \frac{L_k}{\bar{v}_k^2} \frac{\partial \bar{v}_k}{\partial x_k} - \frac{L_{k+1}}{\bar{v}_{k+1}^2} \frac{\partial \bar{v}_{k+1}}{\partial x_k} \quad (31)$$

where

$$\frac{\partial L_k}{\partial x_k} = \frac{x_k - x_{k-1}}{L_k} \quad (32)$$

$$\frac{\partial L_{k+1}}{\partial x_k} = \frac{x_k - x_{k+1}}{L_{k+1}} \quad (33)$$

and

$$\frac{\partial \bar{v}_k}{\partial x_k} = \frac{\partial \bar{v}_{k+1}}{\partial x_k} = \frac{1}{2} \frac{\partial v_k}{\partial x_k} \quad (34)$$

This gives a tri-diagonal system of equations of the form:

$$a_k x_{k-1} + b_k x_k + c_k x_{k+1} = r_k \quad (35)$$

which, after combining it with similar equations for y_k and z_k is extremely fast and efficient to solve. (31) is not exactly linear, since a relocation of the nodes may change the average velocity \bar{v}_k , but we find that it iterates quickly to a minimum.

An appropriate local velocity model to test these results is a model based on refraction seismic experiments around Mount Vesuvius (Lomax, pers. comm., 1999). A slightly smoothed version of this model is shown in Figure 6. Note that at shallow depth the velocity variations approach 100%. The structure below 4 km depth is much more homogeneous.

The algorithm to solve the ray tracing equations has no difficulty with this extreme velocity structure. Figure 7 shows the travel time field in the plane $z = 0$ for a source at the surface, west of Vesuvius.

As can be seen from (22), the computation of the travel time field from every source and every receiver gives us the required delay times to use in (24). Of course, we also need the geometrical spreading. For this, we used the expression (Dahlen and Tromp, 1998, eq. 12.27):

$$\mathcal{R}_{xs} = \sqrt{\frac{|d\Sigma_x|}{d\Omega_s}} \quad (36)$$

where $d\Omega_s$ is the solid angle at the source s spanned by four rays next to the central ray in orthogonal directions, and where $|d\Sigma_x|$ is the cross-sectional area spanned by these rays at the model point x of interest. A careful balance must be struck between choosing a large solid angle $d\Omega$ with a stable estimate of \mathcal{R} that averages out many of the spatial fluctuations in amplitude, or a more localized estimate that suffers a

larger numerical error. Since wavefront healing affects wave amplitudes as well we are permitted to choose wider angles, but if the ray tubes for different central rays overlap we may violate energy conservation. We investigated the accuracy of \mathcal{R} by testing reciprocity for the Vesuvius model and conclude that errors of the order of 10% are common. Such errors, while large, lead only to a second order error in the Fréchet kernels and are considered acceptable for our purpose, but efforts to improve on the efficient computation of \mathcal{R} are ongoing (Nolet and Virieux, work in prep.).

Figures 8–9 show Fréchet kernels for the Vesuvius model. The dominant frequency here is 10 Hz. This is slightly optimistic, since the observed frequencies during the TOMOVES refraction experiment were generally not higher than about 7 Hz (J. Virieux, pers. comm. 2003). Yet, we see that the size of the traveltime and amplitude kernels are large, with a width of 2–3 km: larger than many of the features one would hope to resolve. What the banana-doughnut kernels allow one to do is correct for the wavefront healing induced by the large width of the kernels. There is one caveat, though. If traveltime anomalies heal towards zero at large distances (i.e., towards the right in Figure 5), attempts to interpret them using the banana-doughnut kernels are akin to inverting a diffraction equation, which is notoriously unstable (Nolet and Dahlen, 2000). One can understand this intuitively, because at large distance, a strong velocity anomaly gives only a small travel time delay. Inverting this involves multiplying the small delay by large numbers, running the risk that errors in the observation are magnified at the same time. Proper regularization is therefore an important prerequisite for finite-frequency inversions.

Acknowledgments. The authors gratefully acknowledge support for the research reported in this paper from NSF grants EAR0105387 (TD and RM) and EAR0309298 (GN and RM).

References

- Aki, K. and Richards, P.G., *Quantitative Seismology, Vol. 1*, Freeman, New York, 557 pp., 1980.
- Baig, A.M. and F.A. Dahlen, Statistics of traveltimes and amplitudes in random media, *Geophys. J. Int.* 158, 187-210, 2003.
- Bates, C.C., T.F. Gaskell and R.B. Price, *Geophysics in the Affairs of Man*, Pergamon Press, Oxford, 492 pp., 1982.
- Bolton, H. and G. Masters, Travel times of P and S from global digital seismic networks: Implication for the rel-

- ative P and S velocity in the mantle, *J. Geophys. Res.* **106**, 13527–13540, 2001.
- Cerveny, V. and J.E.P. Soares, Fresnel volume ray tracing, *Geophysics* **57**, 902–915, 1992.
- Dahlen, F.A. and A.M. Baig, Fréchet kernels for body wave amplitudes, *Geophys. J. Int.* **150**, 440–466, 2002.
- Dahlen, F.A., S.-H. Hung and G. Nolet, Fréchet kernels for finite-frequency traveltimes – I. Theory, *Geophys. J. Int.* **141**, 157–174, 2000.
- Dahlen, F.A. and J. Tromp, *Theoretical Global Seismology*, Princeton Univ. Press, Princeton NJ, 1025 pp., 1998.
- Favier, N., S. Chevrot and D. Komatitsch, Near-field influence on shear wave splitting and traveltime sensitivity kernels, *Geophys. J. Int.* **156**, 467–482, 2004.
- Hung, S.-H., F.A. Dahlen and G. Nolet, Fréchet kernels for finite-frequency traveltimes – II. Examples, *Geophys. J. Int.* **141**, 175–203, 2000.
- Hung, S.-H., F.A. Dahlen and G. Nolet, Wavefront healing: a banana-doughnut perspective, *Geophys. J. Int.* **146**, 289–312, 2001.
- Li X.-D. and T. Tanimoto, Waveforms of long-period body waves in a slightly aspherical Earth model, *Geophys. J. Int.* **112**, 92–102, 1993.
- Li X.-D. and B. Romanowicz, Comparison of global waveform inversions with and without considering cross-branch modal coupling, *Geophys. J. Int.* **121**, 695–709, 1995.
- Luo, Y. and G.T. Schuster, Wave-equation travel time tomography, *Geophysics* **56**, 645–653, 1991.
- Marquering, H., R. Snieder and G. Nolet, Waveform inversions and the significance of surface wave modes coupling, *Geophys. J. Int.*, **124**, 258–278, 1996.
- Marquering, H., F.A. Dahlen and G. Nolet, The body wave travel time paradox: bananas doughnuts and 3-D delay-time kernels, *Geophys. J. Int.*, **137**, 805–815, 1999.
- Montelli, R., *Seismic tomography beyond ray theory*, PhD thesis, Princeton University, 207pp., 2003.
- Montelli, R., G. Nolet, G. Masters, F.A. Dahlen and S.H.-Hung, P and PP global travel time tomography: Rays versus waves, *Geophys. J. Int.*, **158**, 637–654, 2004a.
- Montelli, R., G. Nolet, F.A. Dahlen, G. Masters, E.R. Engdahl and S.H.-Hung, Finite-frequency tomography reveals a variety of plumes in the mantle, *Science* **303**, 338–343, 2004b.
- Moser, T.J., Shortest path calculations of seismic rays, *Geophys. J.* **56**, 59–67, 1991.
- Moser, T.J., G. Nolet and R. Snieder, Ray bending revisited, *Bull. Seism. Soc. Am.*, **82**, 259–288, 1992.
- Nolet, G., Imaging the deep earth: technical possibilities and theoretical limitations, in: Roca, A. (ed.), *Proc. XXIIth Assembly ESC, Barcelona 1990*, 107–115, 1992.
- Nolet, G., S.P. Grand and B.L.N. Kennett, Seismic heterogeneity in the upper mantle, *J. geophys. Res.* **99**, 23753–23766, 1994.
- Nolet, G., J.van Trier and R.Huisman, A formalism for nonlinear inversion of seismic surface waves, *Geophys. Res. Lett.* **13**, 26–29, 1986.
- VanDecar, J.C. and R.S. Crosson, Determination of teleseismic relative phase arrival times using multi-channel cross-correlation and least squares, *Bull. Seism. Soc. Am.*, **80**, 150–169, 1990.
- Wielandt, E., On the validity of the ray approximation for interpreting delay times, in: Nolet, G. (ed.), *Seismic Tomography*, 85–98, Reidel Publ. Comp., 1987.
- Woodhouse, J.H. and Girnius, T.P., 1982. Surface waves and free oscillations in a regionalized earth model. *Geophys. J. R. astr. Soc.*, **68**, 653–674.
- Woodward, R.L., and G. Masters, Global upper mantle structure from long-period differential travel times, *J. Geophys. Res.* **96**, 6351–6378, 1991.
- Woodward, M.J., Wave-equation tomography, *Geophys. J.* **57**, 15–26, 1993.
- Wu, R.S. and K. Aki, Scattering characteristics of elastic waves by an elastic heterogeneity, *Geophys. J.* **50**, 582–595, 1985.
- Yomogida, K., Fresnel zone inversion for lateral heterogeneities in the Earth, *Pageoph* **138**, 391–406, 1992.
- Zhao Li, T. H. Jordan and C. H. Chapman, Three-dimensional Fréchet differential kernels for seismic delay times, *Geophys. J. Int.* **141**, 558–576, 2000.

Guust Nolet, F.A. Dahlen and Raffaella Montelli,
Department of Geosciences, Princeton University, Princeton, NJ 08544, USA. (e-mail: nolet@princeton.edu)

Received XX; revised XX; accepted XX.

This preprint was prepared with AGU's L^AT_EX macros v5.01. File paper3p formatted February 23, 2005.

Figure 1. This cartoon illustrates how Born theory works in a homogeneous medium. A wave u' is scattered off a point scatterer and generates a small perturbation u'' that adds to the direct wave u .

Figure 2. The location of the maximum of the cross-correlation of a perturbed wave $u(t) + \delta u(t)$ with the unperturbed $u(t)$ is either advanced (a) or delayed (b), depending on the sign of the scattered wave despite the fact that the latter always is delayed (see text for discussion). Dots denote the location of the maxima in the cross-correlation.

Figure 3. If the scattered wave $\delta u(t)$ has no delay because the heterogeneity is located *on* the raypath, only the amplitude of $u(t)$ is affected

Figure 4. Two examples of kernels for long period (20 s) teleseismic P waves in the Earth's mantle. The kernel in the Northern hemisphere is for a surface reflected PP wave at $\Delta = 120^\circ$, the shorter kernel in the Southern hemisphere for a P wave at 60° . Darker colours indicate more negative values of the kernel, the whitish regions have a positive value for the kernel, implying a positive delay for a positive velocity perturbation. Such 'reverse' sensitivities are located in the second Fresnel zone. Note the region of reduced sensitivity at the center of the kernels, except near the reflection point of PP. The extra complexity of the PP kernel is caused by a 90° phase shift at the caustic, as well as by the fact that scattered waves may also reflect from the surface. The dark shading of the Earth's core does not indicate a sensitivity.

Figure 5. Evolution of body-wave delay times along a ray traversing the center of a spherical anomaly, as a function of the distance x traveled past the anomaly, scaled by the halfwidth L of the anomaly. The three curves are for different values of the halfwidth-to-wavelength ratio L/λ . The initial delay in each case is τ_{\max} . From *Nolet and Dahlen* [2000].

Figure 6. The 3D velocity model for the structure under Mount Vesuvius. Anticlockwise from top left: an E-W vertical cross section, a N-S vertical cross section, and a map view at a depth of 500 m.

Figure 7. (left) Travel time field at $z = 0$ for a source located 10 km west of the summit of Vesuvius, (right) the value of \mathcal{R} for the same configuration.

Figure 8. Travel time Fréchet kernel for a 10 Hz wave passing beneath Mount Vesuvius. Units are s/km^3

Figure 9. Amplitude Fréchet kernel for a 10 Hz wave passing beneath Mount Vesuvius. Units are km^{-3}

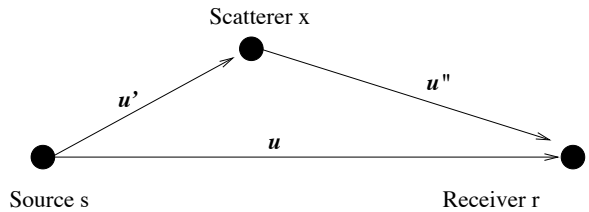


Figure 1: This cartoon illustrates how Born theory works in a homogeneous medium. A wave u' is scattered off a point scatterer and generates a small perturbation u'' that adds to the direct wave u .

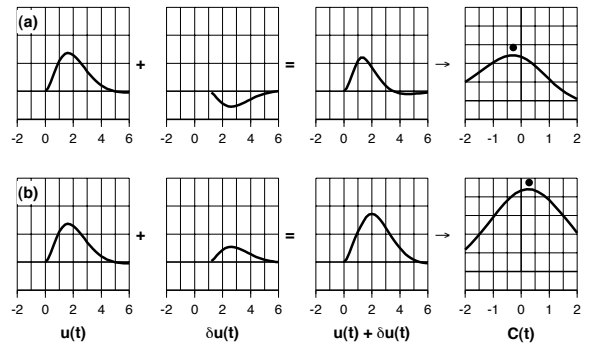


Figure 2: The location of the maximum of the cross-correlation of a perturbed wave $u(t) + \delta u(t)$ with the unperturbed $u(t)$ is either advanced (a) or delayed (b), depending on the sign of the scattered wave despite the fact that the latter always is delayed (see text for discussion). Dots denote the location of the maxima in the cross-correlation.

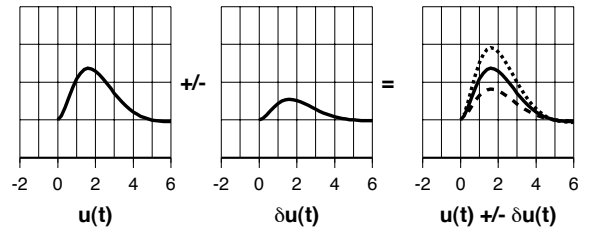


Figure 3: If the scattered wave $\delta u(t)$ has no delay because the heterogeneity is located *on* the raypath, only the amplitude of $u(t)$ is affected

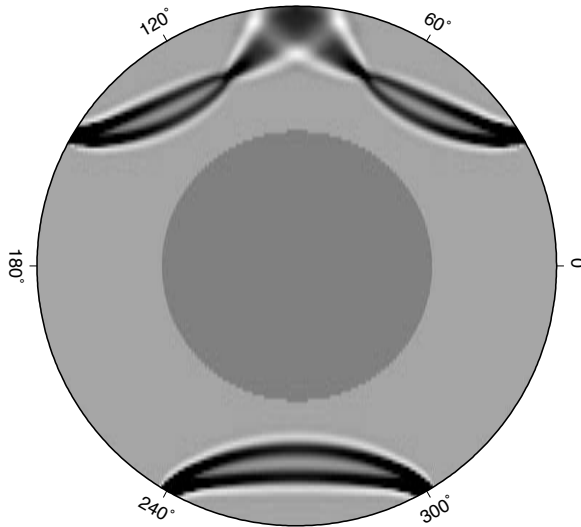


Figure 4: Two examples of kernels for long period (20 s) teleseismic P waves in the Earth's mantle. The kernel in the Northern hemisphere is for a surface reflected PP wave at $\Delta = 120^\circ$, the shorter kernel in the Southern hemisphere for a P wave at 60° . Darker colours indicate more negative values of the kernel, the whitish regions have a positive value for the kernel, implying a positive delay for a positive velocity perturbation. Such 'reverse' sensitivities are located in the second Fresnel zone. Note the region of reduced sensitivity at the center of the kernels, except near the reflection point of PP. The extra complexity of the PP kernel is caused by a 90° phase shift at the caustic, as well as by the fact that scattered waves may also reflect from the surface. The dark shading of the Earth's core does not indicate a sensitivity.

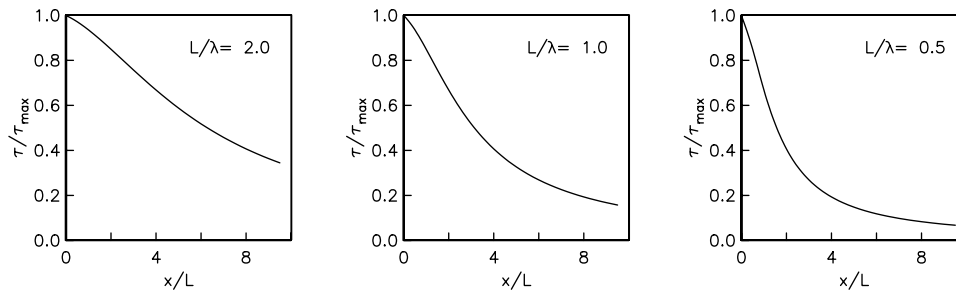


Figure 5: Evolution of body-wave delay times along a ray traversing the center of a spherical anomaly, as a function of the distance x traveled past the anomaly, scaled by the halfwidth L of the anomaly. The three curves are for different values of the halfwidth-to-wavelength ratio L/λ . The initial delay in each case is τ_{\max} . From *Nolet and Dahlen* [2000].

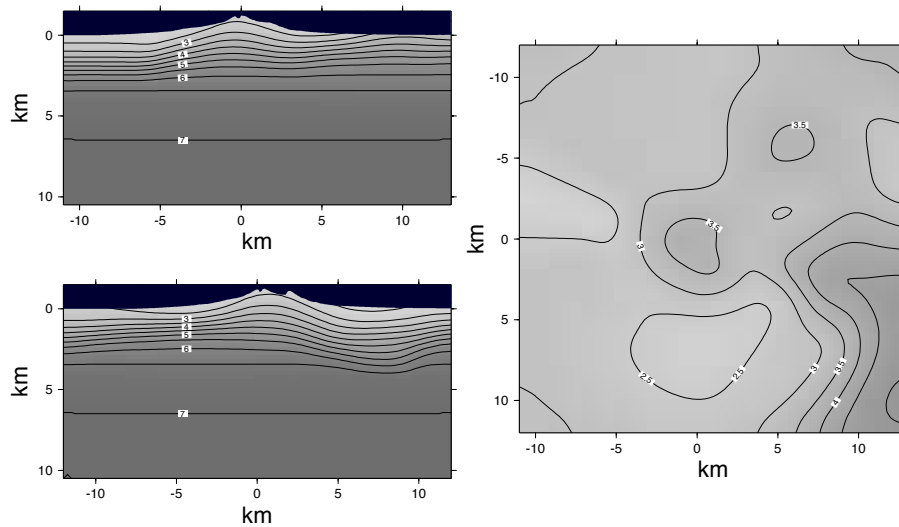


Figure 6: The 3D velocity model for the structure under Mount Vesuvius. Anticlockwise from top left: an E-W vertical cross section, a N-S vertical cross section, and a map view at a depth of 500 m.

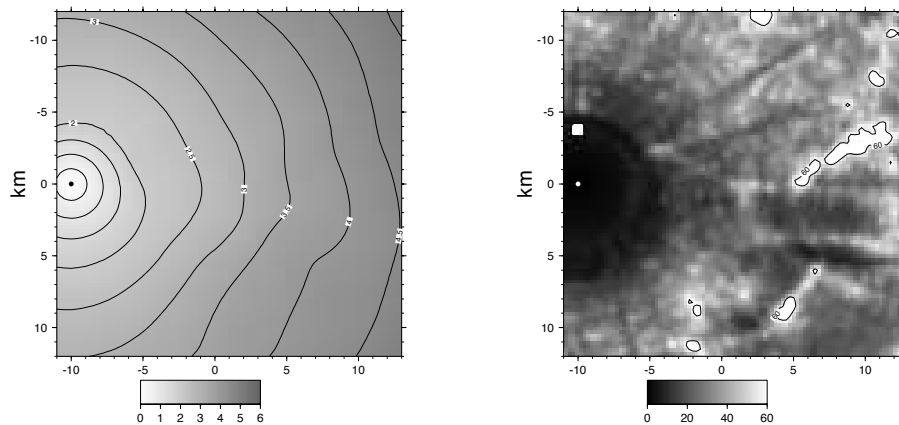


Figure 7: (left) Travel time field at $z = 0$ for a source located 10 km west of the summit of Vesuvius, (right) the value of \mathcal{R} for the same configuration.

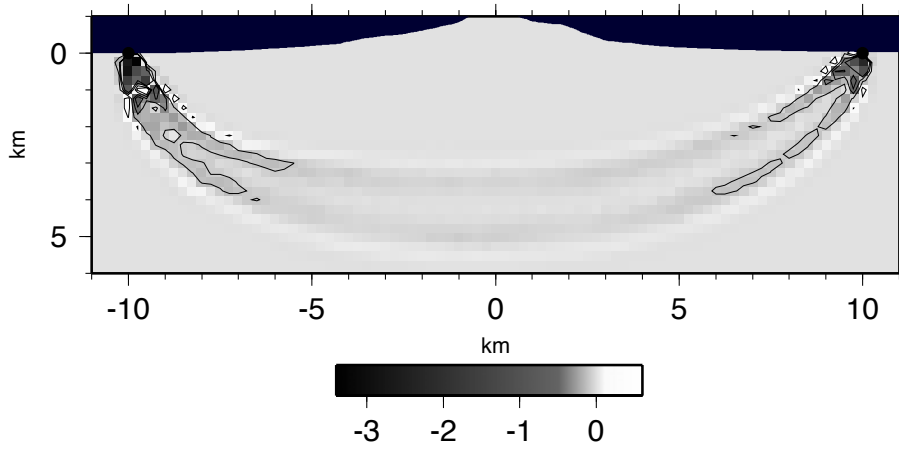


Figure 8: Travel time Fréchet kernel for a 10 Hz wave passing beneath Mount Vesuvius. Units are s/km^3

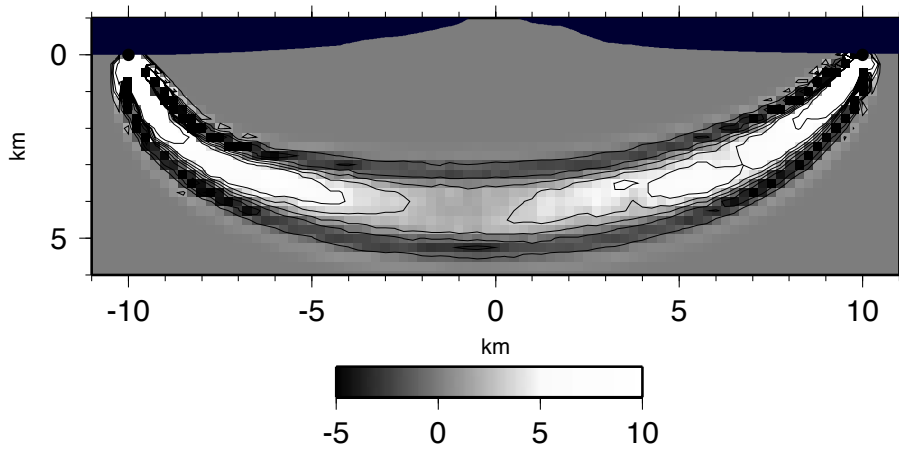


Figure 9: Amplitude Fréchet kernel for a 10 Hz wave passing beneath Mount Vesuvius. Units are km^{-3}